Experimental density data of three carbon dioxide and oxygen binary mixtures at temperatures from 276 to 416 K and at pressures up to 20 MPa

Snaide Ahamada[a], Alain Valtz[a], Salaheddine Chabab[a], Laura Blanco-Martín[b], Christophe Coquelet[a]

a MINES ParisTech PSL University, CTP-Centre of Thermodynamics of Processes, 35, Rue Saint Honoré, 77305 Fontainebleau, France

b MINES ParisTech PSL University, Department of Geosciences, 35, Rue Saint Honoré, 77305 Fontainebleau, France

** Corresponding Author: Christophe Coquelet (Christophe.coquelet@mines-paristech.fr)*

Tel: +33164694962 Fax: +33164694968

ABSTRACT

In the context of Power-to-Gas systems, including Power-to-Gas–Oxyfuel, possible storage of a mixture of CO_2 and O_2 requires density data information and evaluation of equations of state. Densities of three CO_2-O_2 binary system were measured using a vibrating tube densitometer (VTD), and the forced path mechanical calibration (FPMC) method in the gas, liquid and supercritical regions between 276 and 416 K and at pressures up to 20 MPa (maximum expanded uncertainties $U(p)$= 0.0005 MPa, $U(T)$= 0.3 K and $U(\rho)$= 15 kg.m^{-3}). The mole fractions of the prepared CO_2/O_2 mixtures are 0.726/0.274, 0.517/0.483 and 0.872/0.128. The Peng-Robinson cubic equation of state (PR EoS) and the EoS-CG, based on GERG-2008 (and implemented in Refprop v10.0), were considered for the analysis of the data. Comparisons were done with literature data. It appears that the data are overall better predicted by the EoS-CG than the PR EoS.

List of symbols

a	Parameter of the Peng-Robinson equation of state (attractive parameter) [Pa.m^6.mol^{-2}]
b	Parameter of the Peng-Robinson equation of state (co volume parameter) [m^3.mol^{-1}]
C_{ij}	NRTL model binary interaction parameter (Eq. 6) [J.mol^{-1}]
g	molar Gibbs free energy [J.mol^{-1}]
Fobj	Objective function
p	Pressure [MPa]
R	Gas constant [J.mol^{-1} K^{-1}]
T	Temperature [K]
Z	Compressibility factor
x	Liquid mole fraction
y	Vapor mole fraction
N	Number of components

Greek letters

α	Peng-Robinson equation of state alpha function

α_{ij}	NRTL model parameter (Eq. 6)
ω	Acentric factor
Δ	Deviation

Superscript

E	Excess property

Subscripts

C	Critical property
cal	Calculated property
exp	Experimental property
i,j	Molecular species
v	Vapor phase
l	liquid phase

1. Introduction

In the context of energy transition from fossil to low-carbon energy, the Power-to-Gas concept seems to be a very promising solution[1]. It consists of a transformation of CO_2 with H_2, produced by water electrolysis using renewable electricity, into methane, CH_4 (methanation: Sabatier reaction). Methane can be used as a fuel or can be transformed into electricity (oxyfuel combustion for example[2]). Due to the intermittent nature of renewable sources of energy like solar or wind, it is important to develop solutions for massive energy storage. Massive energy storage is necessary to succeed in the energy transition and a solution consists of storage in salt caverns. The design of salt caverns requires thermodynamic properties such as gas solubility in brine and also volumetric properties of the stored products. In Power-to-Gas–Oxyfuel, storage of CO_2, O_2 and CH_4 is required. In general, products are stored in single-phase conditions in salt caverns, but in the case of CO_2, phase changes are possible as its critical pressure and temperature are in the range of typical storage conditions. In order to overcome the problem, one solution would be to mix CO_2 and O_2 in the same salt cavern [3]. As O_2 is a cryogenic fluid, a mixture of CO_2 with O_2 will lead to a lower value of critical temperature. This way the mixture will stay in single-phase conditions.

It exists several sets of data in the open literature concerning the density of mixtures of CO_2 and O_2. Li et al.[4] have published in 2019 a very complete review concerning the available thermo-physical properties of CO_2 mixtures.in the context of CO_2 capture and storage (CCS). They have mentioned in their paper all the available references concerning the VLE and density properties of the CO_2+O_2 binary system. We can also cite the works of Lozano–Martín et al.[5], Commodore et al.[6] and Mantovani et al.[7]. In these investigations, the composition in O_2 is lower than 0.2.

In this work, the densities of three CO_2-O_2 mixtures were measured using Vibrating Tube Densitometer (VTD) in the gas, liquid and supercritical regions. A wide range of O_2 molar fractions was investigated. The measurements were carried out at eight isotherms between 276 and 416 K at pressures up to 20 MPa. The measured densities were also employed to evaluate the capability of a cubic Equation of State (EoS) to predict the density of the binary mixtures. The cubic EoS is composed of the Peng-Robinson (PR-EoS) associated with a g^E mixing rule. Additionally, a recent EoS based on GERG-2008, EOS-CG[8], was evaluated using the measured density data and derived thermodynamic properties (compressibility factor). The experimental data obtained successfully compares to available density data in the literature.

2. Experimental part

2.1. Materials

CO_2 and O_2 were purchased from Air Liquide with a purity higher than 99.995 vol.% and 99.999 vol.% (Table 1). Table 2 presents the exact composition of the three mixtures. The mixtures were prepared in a gas reservoir considering the difference of total pressure. CO_2 was first introduced into the gas reservoir under vacuum. Pressure was recorded (*P1*). Afterwards, O_2 is introduced and pressure is recorded (*P2*). The temperature of the gas reservoir is selected in order to have a monophasic phase inside. Approximate composition is estimated using $x_{O2}=(P2-P1)/P2$.

For more accuracy, the compositions were determined by means of a Gas Chromatograph analysis (Varian, model CP 3800), using a thermal conductivity detector (TCD). WINILAB III software (Perichrom, France) is used for peaks integration and their analysis. The calibration of the GC detector is made by introducing known pure component volumes with appropriate syringes. The packed column used in the gas chromatograph is a PORAPAK R (80/100 mesh, 1.2 m X 1/8" Silcosteel) column. A calibration curve between moles number introduced and GC peak surface is determined and considered to estimate the accuracies. The resulting relative accuracies concerning the mole numbers are 1.1% for CO_2 and 1.2 % for O_2 for mixture 2 and 0.7% for CO_2 and 1.6 % for O_2 for mixtures 1 and 3. The uncertainty of molar fractions (x_1) is determined by Eq. (1):

$$u(x_1) = x_1(1-x_1)\sqrt{\left(\frac{u(n_1)}{n_1}\right)^2 + \left(\frac{u(n_2)}{n_2}\right)^2} \quad (1)$$

with $u(x_1)$ the uncertainty on mole fraction for component 1 and $\frac{u(n_i)}{n_i}$ the relative uncertainty on mole number calculated from GC calibration. It should be noticed that type B uncertainty should be considered to calculate relative uncertainties on mole numbers from calibration curves.

Table 1: Chemical samples used for experimental work.

Chemicals	CAS number	Supplier	Purity (mol %)	Analysis method[a]
Carbon dioxide	124-38-9	Air Liquide	99.995	GC
Oxygen	7782-44-7	Air Liquide	99.999	GC

[a] GC: Gas Chromatography

Table 2: Expected composition and real composition mole fractions.

Mixture number	Expected composition mole fractions		Real composition mole fractions		Standard uncertainties
	CO_2	O_2	CO_2	O_2	$u(x_1)$
1	0.7	0.3	0.726	0.274	0.003
2	0.5	0.5	0.517	0.483	0.004
3	0.9	0.1	0.872	0.128	0.002

2.2. Apparatus

The Vibrating Tube Densitometer (VTD), Anton Paar DMA 512P was used to measure the densities. This equipment is similar to that described in previous work by Rivollet et al.[9], Coquelet et al.[10] or Nazeri et al.[11]. Figure 1, from Rivollet et al., presents a schematic diagram of the apparatus.

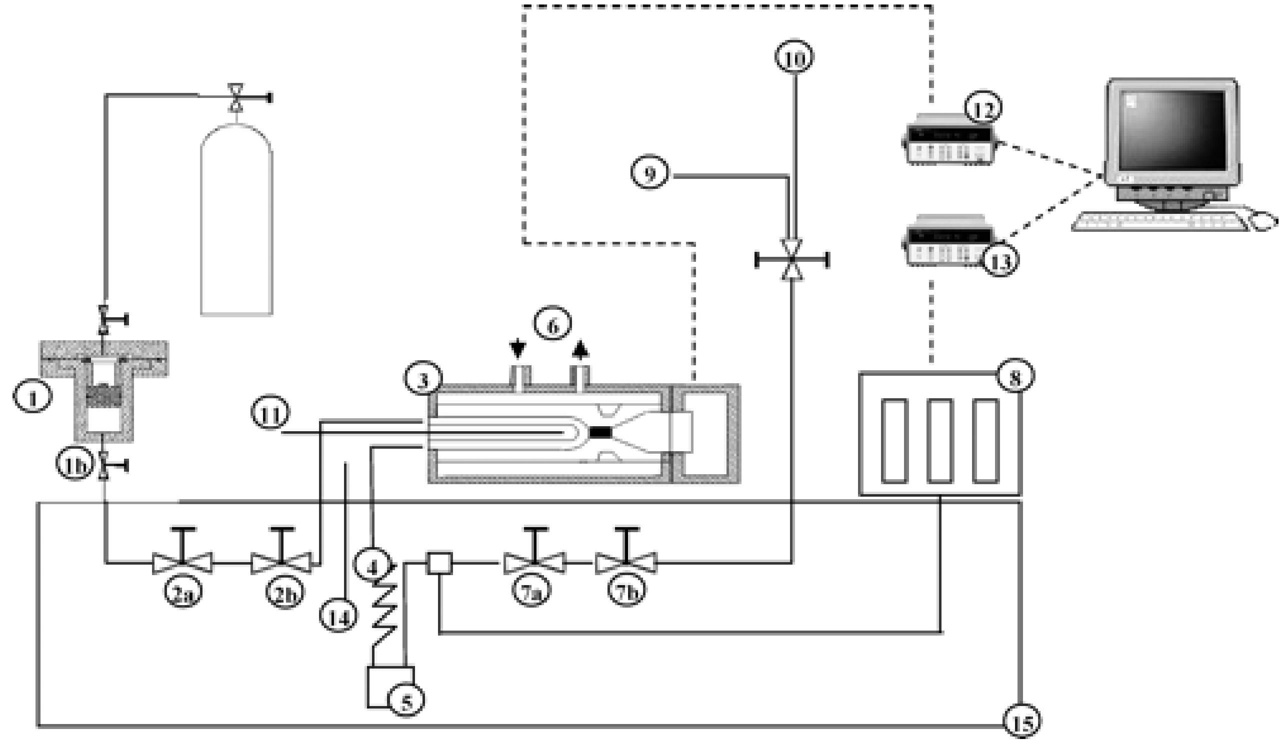

Figure 1: Flow diagram of the equipment, from Rivollet et al.[9]: 1, loading cell; 2a and 2b, regulating and shut-off valves; 3, DMA 512 P densitometer (Anton Paar); 4, heat exchanger; 5, bursting disk; 6, inlet and outlet of the temperature regulating fluid; 7a and 7b, regulating and shut-off valves; 8, pressure sensors maintained at constant temperature (373 K); 9, to vacuum pump; 10, vent; 11, vibrating cell temperature sensor; 12, HP 53131A unit; 13, HP 34970A unit; 14, bath temperature sensor; 15, liquid bath.

The main part of the setup is the U-shaped vibrating tube densitometer provided by Anton Paar. The specifications of the equipment are: pressure up to 140 MPa and temperature between 263 – 473 K. The tube material is made of Hastelloy. The temperature is controlled by fluid (silicon oil Kryo 20 from Lauda, Germany) that circulates in a jacket (small liquid bath) around the densitometer. The temperature stability is ±0.02 K.

The sample fluid is introduced from the gas reservoir into the densitometer through the tube with the diameter of 1.6 mm (1/16 inches) and valves 2. The whole connection tubes are fully immersed in the temperature controlled liquid bath model West P6100. Four-wire 100-Ω platinum resistance probes (Pt100) (PP) measure the temperature at each part of the equipment. The PP were calibrated against the 25-Ω reference thermometer (model: Tinsley Precision Instrument with an uncertainty $u(T)$=0.02 K). The standard uncertainty of the temperature probes was estimated to be $u(T)$ = 0.03 K after calibration. There are two thermostated pressure transducers (PT) of type Druck UNIK 5000 to measure different levels of pressure. PT1 can measure pressures up to 5 MPa, and PT2 can measure pressures up to 40 MPa. The transducers were calibrated using a dead weight tester (model: Desgranges & Huot 5202S) for pressures up to 30 MPa.

The pressure transducers can measure the pressure with the standard uncertainties of $u(p)$ = 0.0003 MPa and $u(p)$ = 0.0005 MPa in the ranges of 0-5 MPa and 5-20 MPa, respectively. The pressure and the temperature were recorded using Agilent HP34970A data acquisition unit and the vibration period, τ, also was recorded using a HP53131A data acquisition unit.

2.3. VTD Calibration and Experimental procedure

The calibration is performed using a reference fluid, CO_2. The forced path mechanical calibration (FPMC) model[12, 13] and the density data predicted by Span and Wagner EoS with measured values of temperature and pressure, implemented in REFPROP 10.0 software[10], were used to tune the unknown parameters in this model at full ranges of pressure for each measured isotherm. The measurement procedure is well described in previous publications (Coquelet et al.[10], Nazeri et al.[11]). Figure 2 shows calibration results with CO_2 at 276.6 and 395.19 K. The FPMC method links period of vibration, density, temperature and pressure.

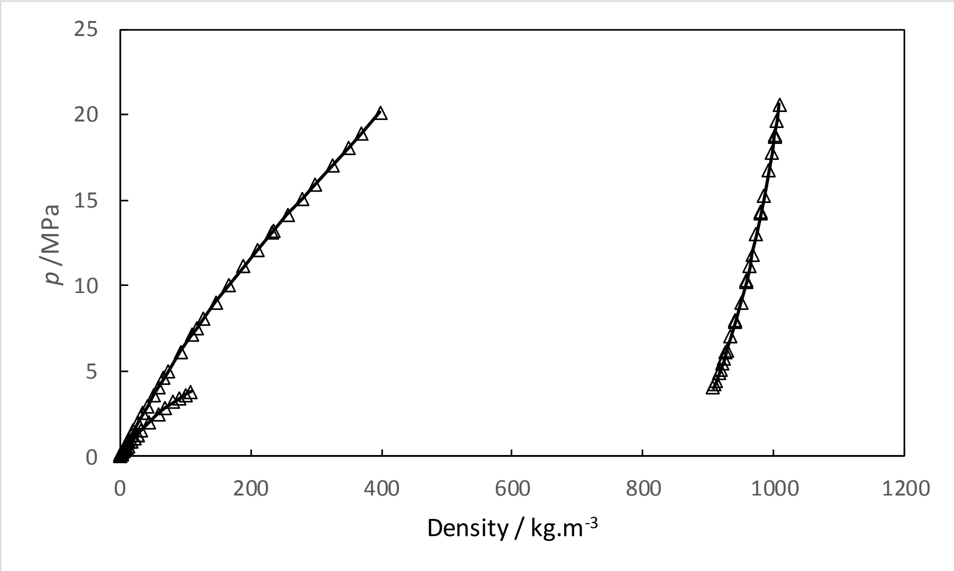

Figure 2: Calibration results with CO_2 at 276.60 and 395.19K. (Δ): density data calculated using Span and Wagner[15] model. Solid line: FPMC[12,13] model.

The experimental procedure is the following. Briefly, vacuum is made in the tube. The fluid mixture is introduced as its gas phase and densities of vapor phase are measured. More fluid mixture is added in order to increase the pressure until the dew pressure. For the liquid density, fluid mixture is added until the maximum pressure (20 MPa). Density measurements are obtained by removing mixture from the VTD (decreasing pressure) until the bubble pressure. In case there is no dew or bubble pressures, starting from vacuum, the fluid mixture is added until the maximum pressure.

It is important to remind that before the appearance of dew point, the temperature of liquid bath is fixed at a value slightly higher than that of the jacket (around the vibrating tube) (difference about 0.2-0.3 °C). It is to be sure that the first drop of fluid mixture appears exactly in the densitometer. In the same manner, before the appearance of bubble point, the temperature of liquid bath is fixed at a value slightly lower than that of the jacket. It is to be sure that the first bubble of fluid mixture appears exactly in the densitometer.

The uncertainties of densities are calculated using Eq. (2) taking into account the calibration with the reference fluid (type B) and repeatability of the measurements (acquisition of the period of vibration). Measurements are made at constant temperature and constant pressure.

$$u(\rho) = \sqrt{\left(\left(\frac{\partial\rho}{\partial p}\right)_{T,x} u(p)\right)^2 + \left(\left(\frac{\partial\rho}{\partial T}\right)_{p,x} u(T)\right)^2 + \left(\sum_i \left(\frac{\partial\rho}{\partial x_i}\right)_{T,p,x_j \neq x_i} u(x_i)\right)^2 + \left(\frac{\alpha}{\sqrt{3}}\right)^2 + u_{rep}^2} \qquad (2)$$

where α represents the maximum of $|\rho_{cal} - \rho_{exp}|$, the difference between the experimental reference fluid (CO_2) density and that calculated by the calibration curve (FPMC method) at the conditions of *T* and *p* and using the reference equation of state from Span and Wagner[15]. u_{rep} is the repeatability of density measurements. Temperature and pressure contributions to density uncertainty are calculated using density derivatives with respect to temperature and pressure of calibration fluid (CO_2) with the Span and Wagner[15] equation of state.

2.4. Experimental Results

The experimental data are presented in Tables 3 to 5.

Table 3: **Experimental isothermal density data for CO_2 +O_2 binary system (Mixture 1: 0.726/0.274) and expanded uncertainties (*k*=2): *U(p)*=0.0003 MPa if *P*<5 MPa and *U*(*p*)=0.0005 MPa if *P*>5 MPa. Italic grey –shaded values correspond to possible metastable states.**

T=276.59 K		*T*= 293.18 K		*T*=313.18 K		*T*=334.78 K		*T*= 353.78 K		*T*=373.46 K		*T*=395.18 K		*T*= 416.38 K	
$U(T)$= 0.06K		$U(T)$= 0.06K		$U(T)$= 0.03K		$U(T)$= 0.04K		$U(T)$= 0.04K		$U(T)$= 0.01K		$U(T)$= 0.02K		$U(T)$= 0.03K	
$U_{min}(\rho)$= 0.2 kg.m^{-3} $U_{max}(\rho)$= 8 kg.m^{-3}		$U_{min}(\rho)$= 0.5 kg.m^{-3} $U_{max}(\rho)$= 15 kg.m^{-3}		$U_{min}(\rho)$= 0.4 kg.m^{-3} $U_{max}(\rho)$= 13 kg.m^{-3}		$U_{min}(\rho)$= 0.1 kg.m^{-3} $U_{max}(\rho)$= 3 kg.m^{-3}		$U_{min}(\rho)$= 0.1 kg.m^{-3} $U_{max}(\rho)$= 3 kg.m^{-3}		$U_{min}(\rho)$= 0.1 kg.m^{-3} $U_{max}(\rho)$= 2 kg.m^{-3}		$U_{min}(\rho)$= 0.2 kg.m^{-3} $U_{max}(\rho)$= 5 kg.m^{-3}		$U_{min}(\rho)$= 0.1kg.m^{-3} $U_{max}(\rho)$= 2.5 kg.m^{-3}	
p/MPa	ρ/kg.m^{-3}	*p*/MPa	ρ/kg.m^{-3}	*p*/MPa	ρ/kg.m^{-3}	*p*/MPa	ρ/kg.m^{-3}	*p*/MPa	ρ/kg.m^{-3}	*p*/MPa	ρ/kg.m^{-3}	*p*/MPa	ρ/kg.m^{-3}	*p*/MPa	ρ/kg.m^{-3}
Vapor phase		1.0261	17.9	1.0370	16.6	1.0254	15.4	1.0148	14.2	1.0219	13.6	1.0606	8.4	1.0645	12.6
0.9987	18.6	1.2667	22.4	1.2480	20.1	1.3693	20.6	1.2659	17.9	1.0250	13.6	1.5114	13.0	1.2566	15.0
1.2970	24.4	1.5059	26.8	1.5210	24.7	1.5113	22.8	1.5263	21.6	1.3410	17.9	2.0356	18.7	1.5084	18.0
1.5079	29.0	2.0296	36.9	2.0296	33.4	2.0228	31.0	1.9712	28.1	1.3688	18.3	2.4969	25.5	2.0063	24.0
2.0233	40.3	2.4379	45.1	2.5489	42.7	2.5291	39.1	2.4979	36.1	1.6226	21.7	3.0690	39.3	2.4614	29.6
2.5375	51.2	3.0468	57.9	3.0567	52.0	3.1154	48.9	3.0511	44.3	1.9322	26.0	3.5236	45.3	2.9955	36.2
3.0077	61.6	3.5789	69.7	3.4973	60.5	3.4998	55.4	3.6661	54.1	2.5360	34.5	4.0275	52.2	3.5505	43.1
3.0136	61.7	4.2899	86.5	4.0055	70.5	4.0317	64.9	4.0456	60.1	3.1352	43.0	4.5200	58.8	4.0714	49.7
3.5122	74.9	4.6668	96.0	4.4811	80.2	4.6096	75.3	4.4690	67.1	3.5451	48.9	5.1207	67.2	4.0949	50.0

3.5278	75.4	5.0075	104.9	5.1405	94.3	5.0500	83.4	5.0535	76.8	3.5736	49.4	5.5301	72.8	4.4386	54.3
4.0151	87.7	5.6455	122.5	5.5938	103.8	5.5832	93.6	5.6069	86.1	4.1283	57.4	5.5619	73.3	5.0657	62.4
4.5495	103.9	6.1151	136.8	6.1023	115.6	6.0711	103.0	6.1721	95.8	4.5213	63.2	6.255	81.3	5.6212	69.7
4.5577	104.1	6.6290	153.2	6.5735	127.0	6.5882	113.5	6.6370	103.8	4.9626	70.1	6.5614	87.5	6.1438	76.3
5.0174	118.2	7.1301	170.3	7.0527	139.1	7.0710	123.3	7.1640	113.4	5.6150	79.9	7.0629	94.8	6.5506	81.6
5.6142	140.2	7.6969	191.3	7.6326	154.4	7.5738	133.8	7.6479	122.3	6.1171	87.8	7.5466	101.8	7.1854	90.0
5.6170	140.3	8.0761	206.6	8.1030	167.4	8.0426	143.8	8.2358	133.6	6.5974	95.4	8.0372	109.0	7.6051	95.6
6.0855	159.3	8.5532	227.7	8.5405	180.1	8.5347	154.2	8.5141	139.0	6.9887	101.7	8.6102	117.8	8.1481	103.0
6.5617	*180.2*	9.0386	251.3	9.0941	196.8	9.1248	168.4	9.1170	150.6	7.5485	110.7	9.0850	124.5	8.6379	109.6
7.0648	*212.1*	9.5283	275.9	9.5589	211.0	9.5279	178.0	9.8112	164.2	8.0059	118.3	9.5294	131.3	9.1100	115.9
7.5345	*237.6*	10.0108	301.3	10.0306	225.6	10.1171	192.3	10.4826	177.8	8.5713	127.7	10.0365	139.0	9.4628	120.7
7.5454	*239.8*	10.4985	329.8	10.4962	240.7	10.5476	203.9	11.1379	191.1	8.5873	128.0	10.5693	147.2	10.1724	130.6
8.762	*276.9*	11.0112	359.2	10.4996	240.9	10.5513	204.0	11.5980	200.6	9.0714	136.2	10.5939	147.6	10.9012	140.6
10.7845	*552.3*	11.4862	387.6	10.9917	257.9	11.0054	214.9	12.1985	213.3	9.0863	136.4	10.9452	153.0	12.0581	156.7
11.0870	*574.2*	11.9968	416.8	10.9961	258.2	11.5894	229.4	12.5279	220.3	9.5341	144.1	11.7240	165.1	13.1753	172.4
11.6098	*586.4*	12.5082	444.7	11.4993	276.8	12.0057	239.9	12.9138	228.9	11.0376	170.5	12.7256	181.0	14.0531	184.8
Liquid phase		13.0310	471.3	11.9899	295.7	12.5677	254.2	13.5977	244.4	12.2323	192.0	13.6496	195.6	14.9349	197.3
12.5564	632.5	13.0168	472.3	12.4999	315.7	12.9861	265.2	14.0973	254.8	12.2374	192.1	14.1742	204.0	16.6896	221.9
13.5475	667.3	13.3725	489.3	12.9650	334.1	13.5110	279.1	14.1058	254.8	13.0519	207.0	14.2085	204.5	17.9826	240.2
14.5748	694.3	14.6538	538.5	13.5010	354.7	14.0864	296.3	14.8020	270.2	14.0469	225.4	15.3271	222.5	18.9390	253.8
15.6302	719.2	14.6416	542.8	14.0319	374.8	14.0934	296.7	15.9300	294.4	14.9435	242.0	16.1060	235.3	20.2738	272.8
16.7981	741.7	14.9744	557.7	14.3690	387.6	14.5085	306.8	16.9908	318.8	15.3993	261.7	16.2034	236.9		
17.7179	755.6	16.0189	589.4	14.9869	408.8	14.9433	321.5	16.9956	318.9	17.0421	281.6	17.2424	253.8		
18.4966	767.6	17.0775	618.3	15.3925	425.7	15.5007	334.6	17.4785	331.1	17.9468	298.4	18.1893	269.1		
20.2495	789.5	17.0630	619.1	15.6194	432.4	15.9823	348.6	18.3694	348.7	18.9235	316.3	19.2014	285.3		
		18.0731	643.4	15.9551	443.5	16.4904	362.1	19.3581	369.9	20.1421	338.8	19.2265	285.7		
		18.9935	662.1	16.4724	459.7	17.0442	376.6	20.4754	394.1	20.1378	338.8	20.2283	301.6		
		20.2968	688.1	16.9899	476.0	17.4992	388.6								
				17.5065	491.2	18.0409	402.6								
				17.5148	491.1	18.5295	414.8								
				17.9399	503.6	18.9942	426.1								

18.4855	517.8	19.5023	438.6
19.0051	531.2	19.9399	449.1
19.4521	543.1	20.3140	457.3
19.4581	543.0		
20.2928	562.5		

Table 4: Experimental isothermal density data for CO_2 +O_2 binary system (mixture 2:0.517/0.483) and expanded uncertainties (k=2):.$U(p)$=0.0003 MPa if P<5 MPa and $U(p)$=0.0005 MPa if P>5 MPa

T=280.63 K		T= 293.92 K		T=313.63 K		T=333.21 K		T= 353.46 K		T=373.60 K		T=395.72 K		T= 412.85 K	
$U(T)$= 0.3K		$U(T)$= 0.2K		$U(T)$= 0.07K		$U(T)$= 0.09K		$U(T)$= 0.06K		$U(T)$= 0.1K		$U(T)$= 0.05K		$U(T)$= 0.1K	
$U_{min}(\rho)$= 0.3 kg.m^{-3} $U_{max}(\rho)$= 9 kg.m^{-3}		$U_{min}(\rho)$= 0.1 kg.m^{-3} $U_{max}(\rho)$= 3 kg.m^{-3}		$U_{min}(\rho)$= 0.1 kg.m^{-3} $U_{max}(\rho)$= 2.7 kg.m^{-3}		$U_{min}(\rho)$= 0.1 kg.m^{-3} $U_{max}(\rho)$= 2.5 kg.m^{-3}		$U_{min}(\rho)$= 0.1 kg.m^{-3} $U_{max}(\rho)$= 2 kg.m^{-3}		$U_{min}(\rho)$= 0.1 kg.m^{-3} $U_{max}(\rho)$= 2 kg.m^{-3}		$U_{min}(\rho)$= 0.5 kg.m^{-3} $U_{max}(\rho)$= 7 kg.m^{-3}		$U_{min}(\rho)$= 0.2kg.m^{-3} $U_{max}(\rho)$= 4 kg.m^{-3}	
p/MPa	ρ/kg.m^{-3}	p/MPa	ρ/kg.m^{-3}	p/MPa	ρ/kg.m^{-3}	p/MPa	ρ/kg.m^{-3}	p/MPa	ρ/kg.m^{-3}	p/MPa	ρ/kg.m^{-3}	p/MPa	ρ/kg.m^{-3}	p/MPa	ρ/kg.m^{-3}
1.0219	17.2	1.0246	16.3	1.0472	15.3	1.0155	14.3	1.0444	13.6	1.0241	12.6	1.0653	12.8	1.0441	11.7
1.3394	22.9	1.2331	19.7	1.2643	18.7	1.2265	17.3	1.2764	16.8	1.2614	15.6	1.2743	15.3	1.2864	14.5
1.6537	28.7	1.5047	24.3	1.5056	22.4	1.5333	21.6	1.5315	20.2	1.5458	19.2	1.5488	18.6	1.5657	17.4
2.0153	35.2	2.0222	33.0	2.0467	30.8	2.0282	28.9	2.0277	26.9	2.0885	26.0	2.0313	24.5	2.0840	23.4
2.5069	44.6	2.5310	41.9	2.6601	40.5	2.5609	36.6	2.5469	34.0	2.5646	32.0	2.5585	31.0	2.5089	28.1
3.0256	54.6	3.0318	50.9	2.6690	40.6	3.0575	43.9	3.0411	40.8	3.5445	44.8	3.0501	37.0	3.0522	34.3
3.5492	64.9	3.5266	60.0	3.0530	46.8	3.5308	51.1	3.5362	47.7	4.0720	51.8	3.5160	42.8	3.5102	39.7
4.0264	75.1	4.1454	71.7	3.5421	54.9	4.0576	59.4	4.0019	54.3	4.5326	57.8	4.0235	49.1	3.5129	39.7
4.5352	86.3	4.7065	82.7	4.0055	62.7	4.5343	67.0	4.5310	61.9	5.0571	64.8	4.5348	55.6	4.0658	46.1
5.0437	97.6	5.2948	94.6	4.5119	71.3	5.0226	75.5	5.0639	69.6	5.6110	72.2	5.0142	61.5	4.5342	51.5
5.5936	110.5	6.1200	112.1	5.0869	81.4	5.6148	85.6	5.6206	77.7	6.5922	85.5	5.6212	69.4	5.0091	57.1
6.0780	122.1	6.8166	127.4	5.5060	88.9	6.1091	93.1	6.0908	84.7	7.0975	92.4	6.1170	75.7	5.5898	63.9
6.5663	134.3	7.2607	137.5	6.1028	99.8	6.5675	100.4	6.6584	93.2	7.5801	99.0	6.5478	81.2	6.1112	70.1
6.9954	145.9	8.0523	156.1	6.1485	100.6	7.1151	109.5	7.1090	100.1	8.0887	106.1	7.1777	89.4	6.1177	70.2
7.5527	161.2	8.5833	169.2	6.1635	100.9	7.5868	117.5	7.6165	107.9	8.5637	112.8	7.5727	94.5	6.5145	74.8
8.0253	174.1	9.4241	190.6	6.5114	107.3	8.0747	126.1	8.1279	115.6	9.0477	119.6	8.0988	101.3	6.5351	75.1

8.6304	192.0	10.1205	208.9	7.1026	118.6	8.5662	134.7	8.5896	122.8	9.5688	126.9	8.5463	107.2	7.0876	81.6
8.6246	192.2	11.5615	248.2	7.1133	118.8	9.0788	143.9	9.1311	131.4	10.0544	133.9	9.0976	114.3	7.5998	87.8
9.0663	205.8	11.5565	248.4	7.6008	128.2	9.5489	152.3	10.0255	145.6	11.0624	148.2	9.5775	120.7	8.0564	93.3
9.6689	224.2	12.0924	263.5	8.1760	139.8	10.0527	161.3	11.0868	162.4	12.0623	162.5	10.1030	127.6	8.5614	99.3
10.0351	235.6	12.0880	263.5	8.2646	141.6	10.5497	170.4	12.0187	177.5	13.0453	176.6	11.0325	140.0	8.5748	99.4
11.0633	269.8	13.2030	295.6	9.5421	167.7	11.0536	179.6	13.0730	194.8	13.9880	190.2	12.1180	154.3	9.0691	105.4
11.0517	270.4	13.1990	295.9	10.0591	178.4	11.5643	189.0	13.0725	194.8	14.8730	202.6	13.0650	167.0	9.5479	111.2
11.9929	303.1	14.0458	319.4	11.0860	200.7	12.0412	198.5	14.0107	210.2	16.0800	220.5	14.0217	179.8	10.0528	117.3
13.0339	340.0	14.0378	319.5	12.1605	224.4	12.5159	207.7	15.0277	226.9	16.0822	220.6	15.1979	195.4	10.8987	127.6
14.0656	376.6	15.0380	348.4	13.0074	243.4	13.0458	217.8	15.9847	243.0	17.0522	235.1	16.2579	209.6	12.1664	142.7
15.0294	410.6	15.0341	348.7	14.316	271.7	13.5555	227.5	17.0015	259.8	17.0555	235.1	17.0434	220.2	13.0663	153.5
16.2689	449.0	16.6414	392.3	14.9472	288.2	13.9996	236.0	18.0245	276.5	17.8714	247.1	18.1289	234.7	14.1484	166.9
16.2619	449.5	16.6354	392.7	15.9882	311.6	14.5189	245.6	18.9421	291.1	19.0095	263.6	19.3526	250.7	16.4731	195.5
16.9518	468.7	17.9488	426.4	16.1772	315.8	15.0036	254.7	20.3158	312.6	19.0090	263.6	20.2032	261.7	17.0456	202.3
16.9476	468.9	17.9420	426.8	17.4641	344.8	15.9818	273.4			20.0154	277.9			18.4366	218.7
18.5980	510.7	19.1108	456.3	18.8837	375.4	16.9748	292.6							20.0959	238.3
18.5864	511.2	20.1976	480.4	20.1692	401.9	18.0141	312.7								
20.3276	553.1			20.1674	401.9	19.0085	331.1								
						19.9326	348.1								
						20.2304	353.8								

Table 5: **Experimental isothermal density data for CO_2 +O_2 binary system (mixture 3: 0.872/0.128) and expanded uncertainties (*k*=2): *U(p)*=0.0003 MPa if *P*<5 MPa and *U(p)*=0.0005 MPa if *P*>5 MPa. Italic grey –shaded values correspond to possible metastable states.**

T=279.05 K		*T*= 293.31 K		*T*=315.06 K		*T*=333.25 K		*T*= 353.62 K		*T*=374.23 K		*T*=394.15 K		*T*= 414.31 K	
U(*T*)= 0.1 K		*U*(*T*)= 0.09K		*U*(*T*)= 0.07K		*U*(*T*)= 0.04K		*U*(*T*)= 0.03K		*U*(*T*)= 0.07K		*U*(*T*)= 0.03K		*U*(*T*)= 0.02K	
Umin(ρ)= 0.3 kg.m^{-3} *Umax*(ρ)= 13 kg.m^{-3}		*Umin* (ρ)= 0.2 kg.m^{-3} *Umax*(ρ)= 9 kg.m-^{3}		*Umin* (ρ)= 0.1 kg.m^{-3} *Umax* (ρ)= 4 kg.m^{-3}		*Umin* (ρ)= 0.1 kg.m^{-3} *Umax* (ρ)= 4 kg.m^{-3}		*Umin* (ρ)= 0.1 kg.m^{-3} *Umax* (ρ)= 3 kg.m^{-3}		*Umin* (ρ)= 0.4 kg.m^{-3} *Umax* (ρ)= 4 kg.m^{-3}		*Umin* (ρ)= 0.1 kg.m^{-3} *Umax* (ρ)= 2.5 kg.m^{-3}		*Umin* (ρ)= 0.1kg.m^{-3} *Umax* (ρ)= 2.5 kg.m^{-3}	
p/MPa	ρ/kg.m^{-3}	*p*/MPa	ρ/kg.m^{-3}	*p*/MPa	ρ/kg.m^{-3}	*p*/MPa	ρ/kg.m^{-3}	*p*/MPa	ρ/kg.m^{-3}	*p*/MPa	ρ/kg.m^{-3}	*p*/MPa	ρ/kg.m^{-3}	*p*/MPa	ρ/kg.m^{-3}
Vapor phase		Vapor phase		1.0407	17.5	1.0219	16.2	1.0073	14.9	1.0273	14.5	1.0665	14.1	1.0140	12.7
1.0416	20.4	1.0043	18.6	1.2437	21.0	1.2800	20.4	1.5203	22.9	1.5180	21.6	1.2007	15.8	1.5137	19.1
1.2633	25.1	1.2769	24.0	1.5758	27.0	1.5362	24.7	2.0373	31.1	2.0810	29.9	1.4843	19.7	2.0358	25.9
1.5048	30.5	1.5412	29.3	1.9996	34.9	2.0297	33.1	2.5328	39.1	2.5194	36.5	2.0318	27.1	2.5355	32.4
2.0163	42.2	2.0404	40.0	2.5358	45.3	2.5422	42.2	3.1299	49.2	2.9868	43.8	2.4654	33.2	3.0494	39.3
2.5130	53.7	2.5863	52.2	3.0392	55.4	3.0561	51.7	3.5407	56.2	3.5699	53.1	3.0207	41.0	3.5748	46.3
3.0151	68.2	3.0629	63.6	3.5599	66.4	3.5237	60.6	4.0393	65.0	4.0447	61.9	3.5575	48.8	4.0597	52.9
3.2625	76.1	3.5193	75.2	4.0532	77.6	4.0380	70.8	4.5088	73.5	4.5060	71.0	3.9505	54.6	4.0584	52.9
3.5074	84.8	4.0205	89.6	4.5274	88.9	4.6668	83.8	5.0562	83.8	5.0295	78.5	4.5499	63.5	4.5645	60.0
3.7587	92.8	4.5284	104.9	5.1645	105.1	5.0349	91.7	5.7330	97.0	5.5493	86.4	5.0643	71.3	5.0419	66.6
4.1541	106.1	5.0349	122.0	5.5868	116.7	5.5930	104.3	6.0705	103.1	6.1195	96.4	6.0782	87.1	5.6518	75.3
4.2843	110.7	5.6098	144.6	6.1369	132.4	6.1099	116.4	6.6522	115.1	6.1232	96.4	6.5320	94.3	6.0878	81.6
4.4095	115.6	6.0892	166.3	6.6193	147.5	6.6518	129.8	7.0612	124.4	6.6065	105.2	7.0752	103.1	6.7675	91.3

4.5645	122.5	6.6721	198.5	7.0621	162.4	6.6534	129.8	7.5756	136.4	7.0261	112.9	7.5136	110.4	8.1022	111.2
4.6561	127.0	6.9584	217.6	7.5584	180.4	7.0752	140.7	7.9620	145.4	7.5889	123.3	8.0078	118.6	8.4669	116.9
4.7489	131.5	7.2267	240.7	8.0728	200.8	7.0789	140.8	8.5421	157.1	8.0379	131.8	8.0843	119.9	9.2081	128.4
4.9287	143.3	7.3480	253.3	8.0775	200.9	7.5828	154.5	9.0142	166.6	8.5729	142.1	8.4884	126.8	10.2145	143.4
5.0117	*148.8*	*7.4496*	*267.7*	8.5480	221.5	8.0965	168.9	9.5589	179.7	9.0370	151.4	8.5278	127.4	11.2972	161.0
5.1070	*157.2*	*7.5519*	*288.0*	9.0717	247.1	8.5662	183.1	10.0558	192.0	10.0876	173.0	8.9956	135.5	11.9586	171.9
5.2149	*167.2*	*7.6842*	*316.2*	9.5412	272.3	8.5678	183.2	10.7222	210.8	10.4917	181.5	9.0607	136.6	12.9289	189.1
5.3002	*172.7*	*7.8201*	*322.8*	9.9982	298.6	9.0560	198.4	11.4360	232.6	11.0366	193.1	9.4928	144.2	13.8057	203.8
5.3906	*177.8*	*7.9261*	*335.4*	10.2212	315.2	9.2307	203.9	12.0510	252.9	11.9161	212.7	9.5248	145.1	14.7433	219.5
5.4920	*186.0*	*8.0564*	*347.0*	10.6028	335.6	9.5275	214.1	12.7049	273.9	12.9049	235.1	10.0376	154.1	16.1194	242.5
5.5824	*200.7*	*8.2371*	*389.9*	10.6898	347.8	9.5288	214.2	13.5401	294.5	14.0828	262.8	10.5522	163.4	17.5173	266.3
5.7402	*223.4*	*8.3445*	*407.1*	11.1620	372.0	9.7922	223.3	13.9400	304.6	14.9868	284.5	11.0513	172.6	18.9761	290.9
5.8086	*225.2*	*8.4536*	*419.9*	11.7107	412.0	9.7998	223.5	13.9358	304.8	16.0138	309.0	11.6063	182.9	20.0204	308.6
5.9850	*591.8*	*8.5411*	*438.2*	12.0508	435.8	10.0180	231.2	14.9049	330.9	16.9216	330.6	12.1181	192.6		
6.1056	*613.0*	*8.6407*	*465.0*	12.4275	465.9	10.2597	239.7	16.1022	367.7	16.9188	330.8	12.5181	200.2		
6.5946	*698.3*	*8.7582*	*506.2*	12.8458	491.0	10.5548	250.6	16.9052	393.3	18.0110	356.3	12.9645	208.8		
7.1041	*712.4*	*8.9342*	*527.1*	13.5490	532.0	11.0228	268.2	18.2172	432.5	18.8901	376.3	14.1039	231.0		
7.9046	*760.2*	*9.5655*	*9.1884*	553.1	558.4	11.4899	287.1	18.1943	433.4	18.8743	376.5	15.0024	248.1		
7.9152	*760.7*	*9.5655*	*590.2*	15.1136	593.3	12.0560	309.8	18.9987	458.0	20.0624	403.0	15.0023	248.1		
Liquid phase		**Liquid phase**		16.0609	625.0	12.3828	326.2	20.1842	490.7			15.9709	267.1		
8.9179	785.7	10.0875	634.7	17.0546	651.5	12.9982	349.8					17.1688	290.7		
8.9302	786.0	11.0317	680.8	18.1689	677.6	13.4962	375.2					18.6716	320.1		
9.5588	798.3	12.0270	716.9	19.2425	697.4	13.9740	391.5					20.2201	350.2		
9.9407	807.3	12.8227	737.6	20.4052	716.7	14.4890	418.9					20.2215	350.4		
10.9404	823.2	13.8256	758.5			15.2235	444.0								
12.1374	838.5	15.0309	779.0			15.6111	459.6								
12.6650	843.9	15.0396	779.0			16.1478	480.1								
13.0291	850.0	16.0513	794.6			16.8926	505.5								
14.5011	864.8	16.7640	803.4			17.9419	539.0								
15.4452	873.2	18.0263	818.7			18.9661	569.3								
16.8885	885.7	18.4149	822.9			20.2278	600.3								

17.9250	894.2	19.4981	833.5
17.9341	894.4	20.1334	838.0
19.0671	902.2	20.1539	837.1
19.8930	906.4		
20.3845	910.7		

3. Correlation and discussions

3.1. Development of PR EoS

We have used a cubic equation of state to compare its density predictions with the experimental data. Cubic equations of state are often used for the design of underground gas reservoirs as they are very easy to solve. The critical temperatures (T_c) and pressures (P_c) and acentric factors (ω) for pure CO_2 and O_2, which are collected from Simulis thermodynamic software (from Prosim, Toulouse, France), are provided in Table 6.

Table 6. Critical properties and acentric factors for Carbone dioxide and Oxygen pure components (Source Simulis thermodynamic software)

Component	T_c/K	P_c/bar	Acentric factor ω
CO_2	304.21	73.83	0.223621
O_2	154.58	50.43	0.0221798

In order to have the best representation of the phase diagrams, we have considered the Peng-Robinson Equation of State[16] (Eq. 3) with the Wong Sandler Mixing rules[17] (Eqs. 4 and 5) involving the NRTL activity coefficient model[18] (Eq. 6). Indeed, as O_2 is a cryogenic component, the phase diagram has the particularity to have a mixture critical point. Cubic EoS have some difficulties to represent accurately the equilibrium properties close to the mixture critical point.

$$\left(P + \frac{a\alpha(T)}{v^2 + 2vb - b^2}\right)(v - b) = RT \tag{3}$$

$$b = \frac{\sum_i \sum_j \left(b - \frac{a}{RT}\right)_{ij}}{1 - \left(\frac{\sum_i x_i \frac{a_i}{b_i}}{RT} + \frac{g_\gamma^E}{CRT}\right)} \tag{4}$$

with $C=\ln(1/2)$

$$b-\frac{a}{RT}=\sum_i\sum_j x_i x_j\left(b-\frac{a}{RT}\right)_{ij} \text{ with } \left(b-\frac{a}{RT}\right)_{ij}=\frac{1}{2}\left[\left(b-\frac{a}{RT}\right)_i+\left(b-\frac{a}{RT}\right)_j\right](1-k_{ij}) \quad (5)$$

$$g_Y^E=\sum_i x_i\sum_j\frac{x_j exp\left(-\alpha_{ij}\frac{C_{ji}}{RT}\right)}{\sum_k exp\left(-\alpha_{ik}\frac{C_{ki}}{RT}\right)}C_{ji} \quad (6)$$

with C_{ii}=0. The value of the non-randomness parameters, α_{ij}, is equal to 0.1. Note that α_{ij} is different from $\alpha(T)$ which is the alpha function of the PR EoS.

In order to adjust the binary interaction parameters (C_{ij} and k_{ij}), we have considered a database of six references presented in Table 7. As all the systems present a mixture critical point, we have just considered an objective function of the bubble pressure (Eq. 7).

$$Fobj=\sum_i^{Ndata}\left(\frac{p_{exp}-p_{cal}}{p_{exp}}\right)^2 \quad (7)$$

All the data were used to fit the binary interaction parameters. We did not consider any temperature dependency of each binary interaction parameter. The obtained values are $C_{12}=479$ J.mol^{-1}, $C_{21}=-216$ J.mol^{-1} and $k_{12}=0.2078$. The performance of the model was assessed by means of the following relative deviations, *AAD U* and *BIAS U*, which are expressed as:

$$AAD\ U=\frac{1}{N}\sum_{i=1}^N\frac{|U_{i,exp}-U_{i,cal}|}{U_{i,exp}} \quad (8)$$

$$BIAS\ U=\frac{1}{N}\sum_{i=1}^N\frac{(U_{i,exp}-U_{i,cal})}{U_{i,exp}} \quad (9)$$

where U is the pressure (p) or the vapor composition (y_1) and N is the number of experimental measurements. Results are presented in Table 8 and Figure 3. As can be seen, when the temperature approaches the critical temperature of CO_2, the model has some difficulties to represent the equilibrium properties. In order to improve the prediction of the phase diagram, we can consider temperature dependent binary interaction parameters, but it is not judicious for density prediction at temperatures higher than the critical temperature of CO_2.

Table 7 : Summary of vapor liquid equilibrium data of the binary system CO_2 + O_2.

Reference	Type of Data	Temperatures
Fredenslund and Sather 1970[19]	*pTxy*	263.15, 273.15 and 283.15
Kaminishi and Toriumi 1966[20]	*pTxy*	253.15, 273.15, 288.15 and 298.15
Muirbrook and Prausnitz 1965[21]	*pTxy*	273.15
Zenner and Dana 1963[22]	*pTxy*	273.15
Lasala et al. 2016[23]	*pTxy*	273.15, 288.15 and 298.15
Westman et al. 2016[24]	*pTxy*	273.09 and 293.08

Table 8: Values of *BIAS*, and *AAD* of pressure and vapor compositions for the different sets of data.

Reference	*T*/K	*BIAS p*/%	*BIAS y*/%	*AAD p*/%	*AAD y*/%
Fredenslund and Sather 1970[19]	263.15	6.1	-1.6	6.1	2.5
	273.15	4.8	-1.7	4.8	2.3
	283.15	8.5	-3.7	8.5	3.7
Kaminishi and Toriumi 1966[20]	253.15	6.9	-7.6	7.8	7.6
	273.15	6.3	-4.4	6.3	4.4
	288.15	5.6	-4.2	5.6	4.2
	298.15	3.5	-2.0	3.5	2.0
Muirbrook and Prausnitz 1965[21]	273.15	5.7	-1.8	5.7	3.4
Zenner and Dana 1963[22]	273.15	4.6	-4.5	5.8	4.7
Lasala et al. 2016[23]	273.15	12.6	-3.8	12.6	3.8
	288.15	6.4	-2.8	6.4	2.8
	298.15	Calculation failed close to mixture critical point			
Westman et al. 2016[24]	273.09	9.8	-3.3	9.8	3.9
	293.08	2.1	-1.2	2.1	1.2

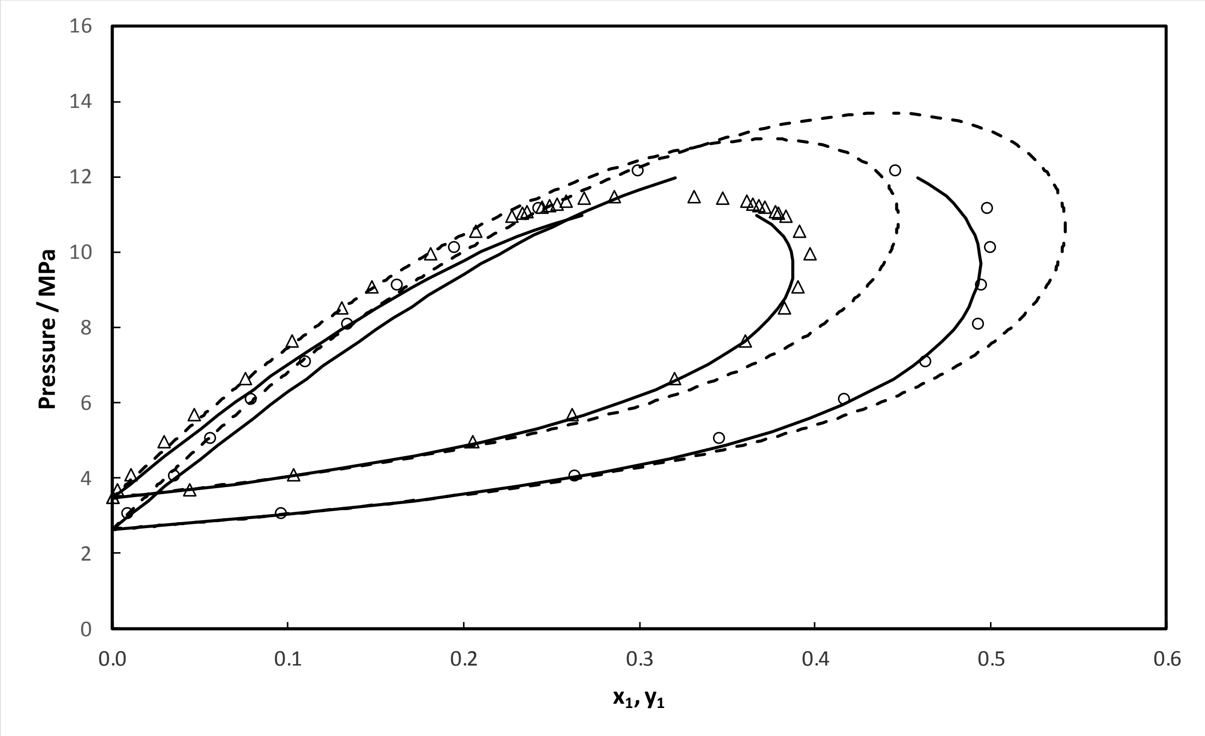

Figure 3 : Vapor – Liquid equilibrium isotherms for O_2 (1) + CO_2 (2) binary system: (Δ): 273.09 K from Westman et al.[24], (o), 263.15 K from Fredenslund and Sather[19]. Solid line: Peng Robinson EoS model, Dashed line: EoS-CG (Gernert and Span[8]) EoS model.

PT envelopes of the three mixtures (see Table 2) are predicted using our thermodynamic model and plotted in Figure 4. In this figure, we have also plotted the *PT* data of each system corresponding to the measured densities. According to Figure 4, we can observe that few density data were determined in the vapor-liquid region. Probably for these data, we are in a metastable state (mixture 3, T=279.05 and 293.31 K, mixture 1, T=276.59 K). These data are mentioned in Tables 3 and 5.

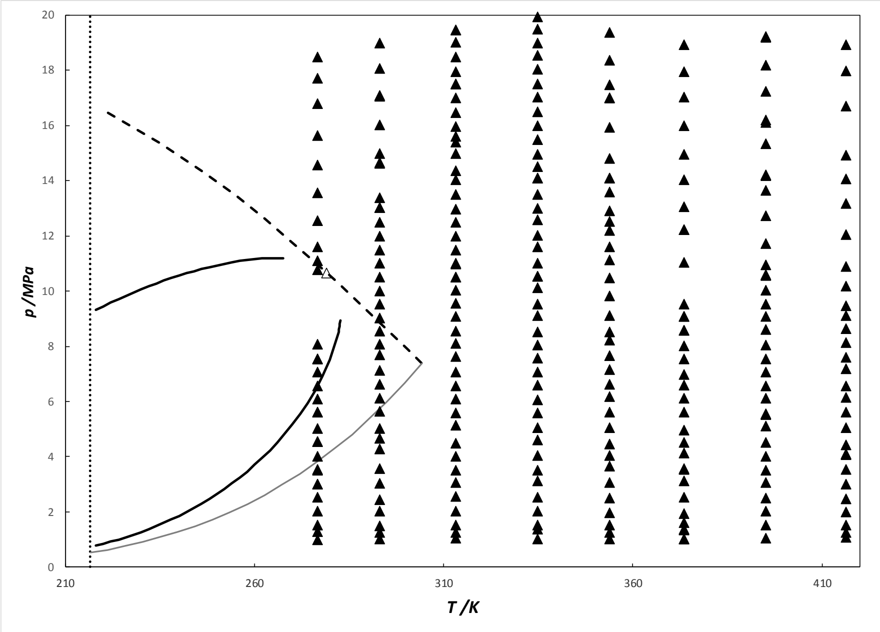
p /MPa
T /K
0
2
4
6
8
10
12
14
16
18
20
210
260
310
360
410

(a)

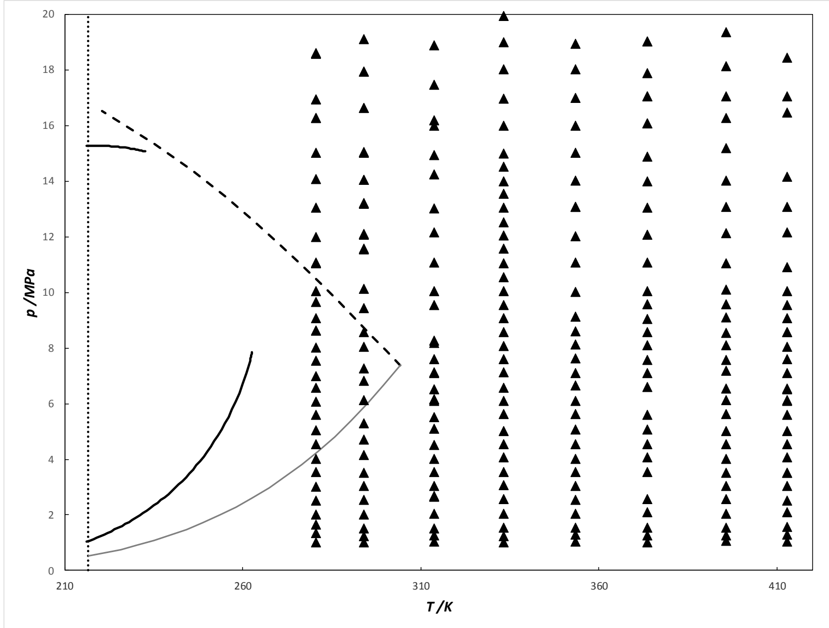
p /MPa
T /K
0
2
4
6
8
10
12
14
16
18
20
210
260
310
360
410

(b)

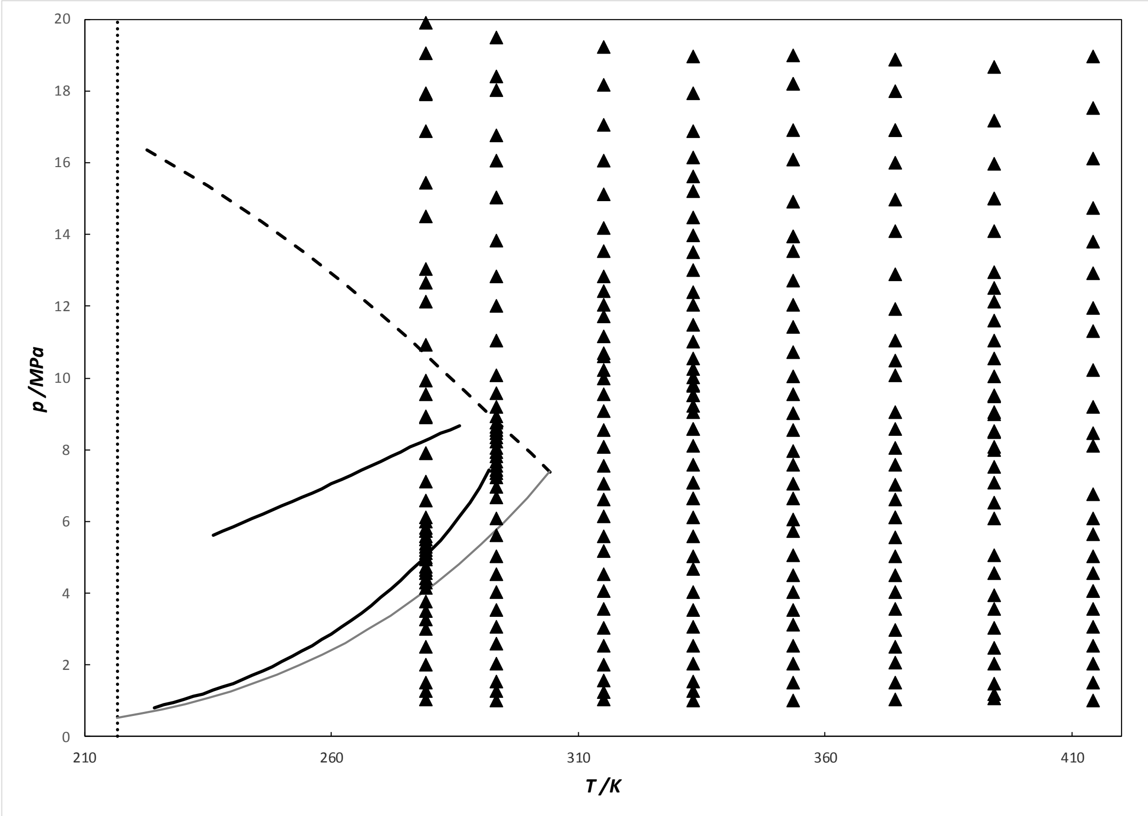

(c)

Figure 4: Pressure Temperature envelope of the CO_2-O_2 binary system calculated using Peng Robinson EoS (compositions listed in Table 2) showing the experimental points measured (▲). (a): Mixture 1, (b): mixture 2, (c): Mixture 3. Grey solid line: Pure CO_2 vapor pressure. Bold dashed line: mixture critical points line.

3.2. Comparison with experimental density data

The PR EoS previously developed is used to predict the experimental data. Table 9 summarizes the *AAD* (Eq. 10) and Maximum Absolute Deviation (*MAD*) in the gas, liquid and supercritical regions. The results (pressure *vs.* molar volume and compressibility factor) for the different mixtures are presented in Figures 5 to 7.

$$AAD\ (\%) = N^{-1} \sum_{i=1}^{N} \left(\left| \rho_{Exp.} - \rho_{Model} \right| / \rho_{Exp.} \right) \times 100 \qquad (10)$$

As it can be seen, the cubic EoS represents the experimental data with satisfactory deviations. As the compressibility factor tends to 1 when the pressure tends to 0 (ideal gas law), it is possible to evaluate the second virial coefficient of the CO_2 – O_2 binary mixture from the measured compressibility factor. Indeed, $Z = 1 + \frac{BP}{RT}$ for low to moderate pressure. It is also a good test to evaluate the consistency of the data at low pressure. In addition, we can observe that the maximum of deviation occurs for the low-pressure measurements ($p < 1.5$ MPa due to VTD precision) and close to bubble or dew points (possible metastable states). As the compressibility depends on the temperature, the density and the pressure, the uncertainties of the compressibility are therefore expressed using Eq. (11). It can be observed that the compressibility factor "concentrates" all the uncertainties of the measurements. The average value of *u(Z)/Z* is around 5%.

$$u(Z) = Z\sqrt{\left(\frac{u(\rho)}{\rho}\right)^2 + \left(\frac{u(T)}{T}\right)^2 + \left(\frac{u(P)}{P}\right)^2} \qquad (11)$$

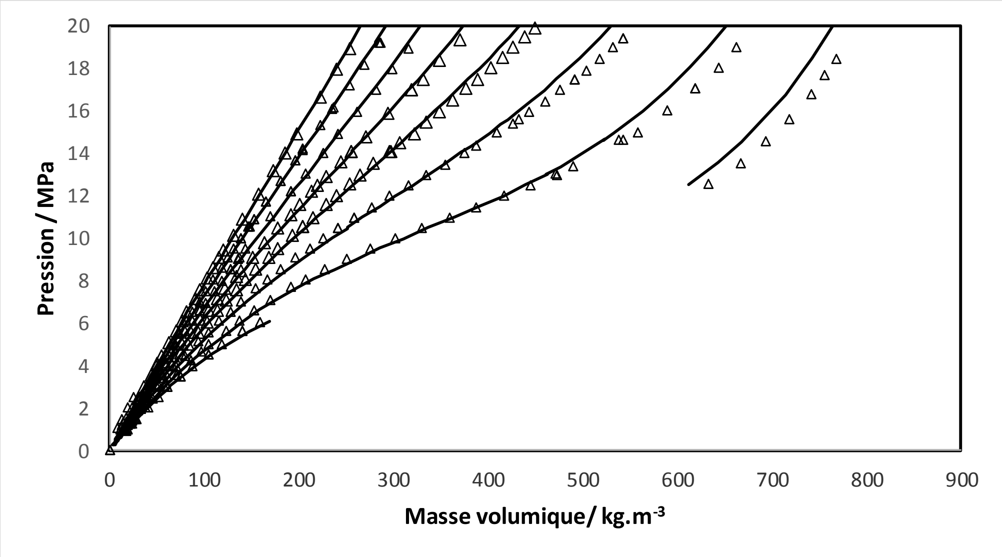

A

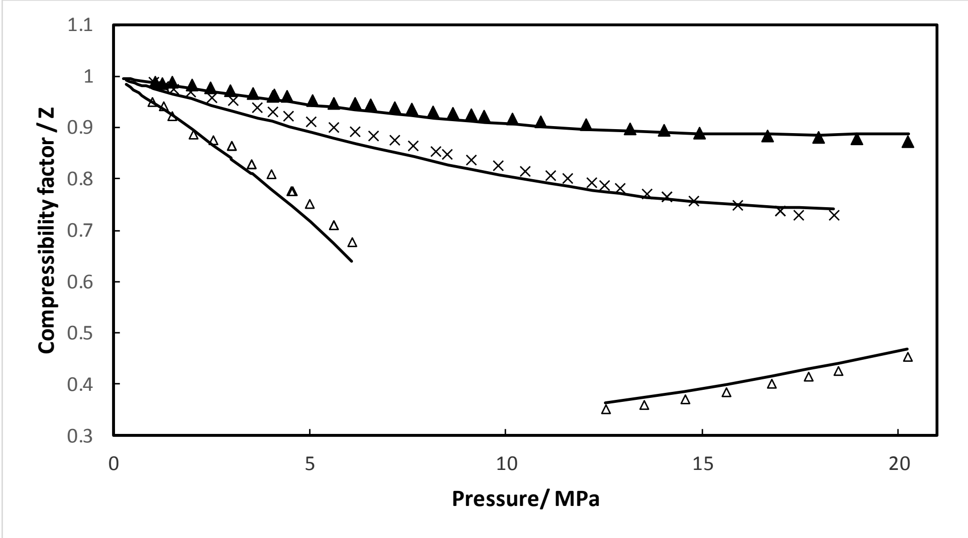

B

Figure 5: A: Pressure as a function of molar density for the O_2 + CO_2 (mixture 1: 0.274/0.726) binary system. B: Compressibility factor as a function of pressure (Δ): 276.59 K, (×): 353.78 K, (▲):416.38 K. Solid line: Peng Robinson EoS with Wong Sandler mixing rules and NRTL Activity coefficient model.

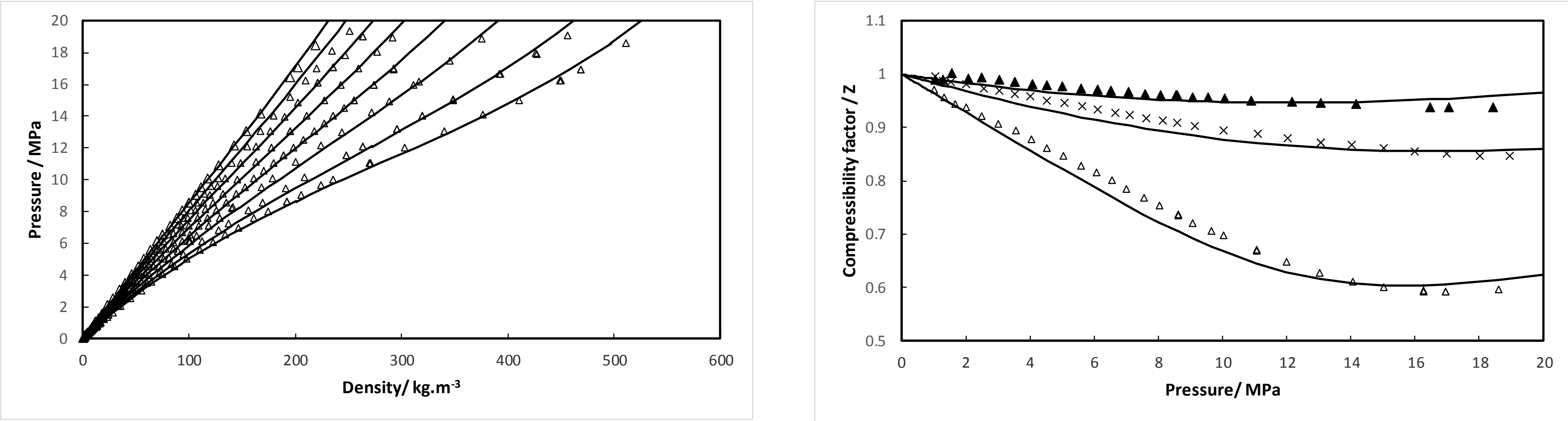

A B

Figure 6: A: Pressure as a function of molar density for the O_2 + CO_2 (mixture 2: 0.483/0.517) binary system. B: Compressibility factor as a function of pressure (Δ): 280.63 K, (×): 353.46 K, (▲):412.85 K. Solid line: Peng Robinson EoS with Wong Sandler mixing rules and NRTL Activity coefficient model.

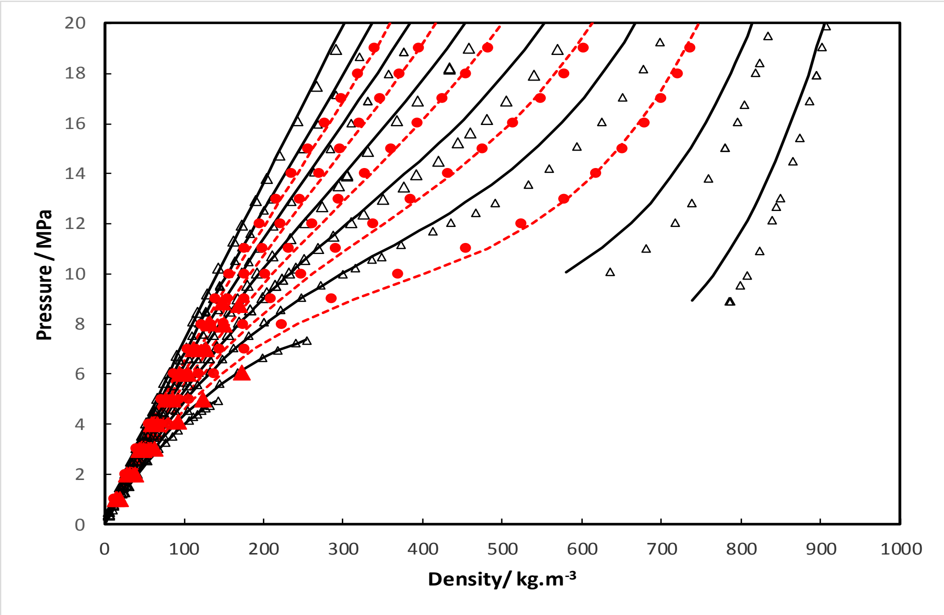

Pressure / MPa
Density/ kg.m-3

A

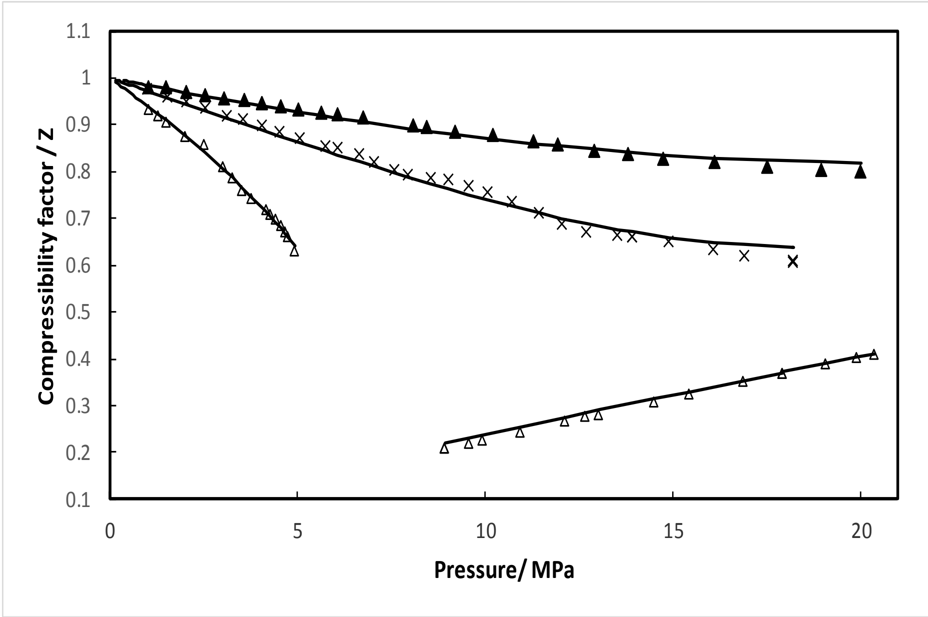

Compressibility factor / Z
Pressure/ MPa

B

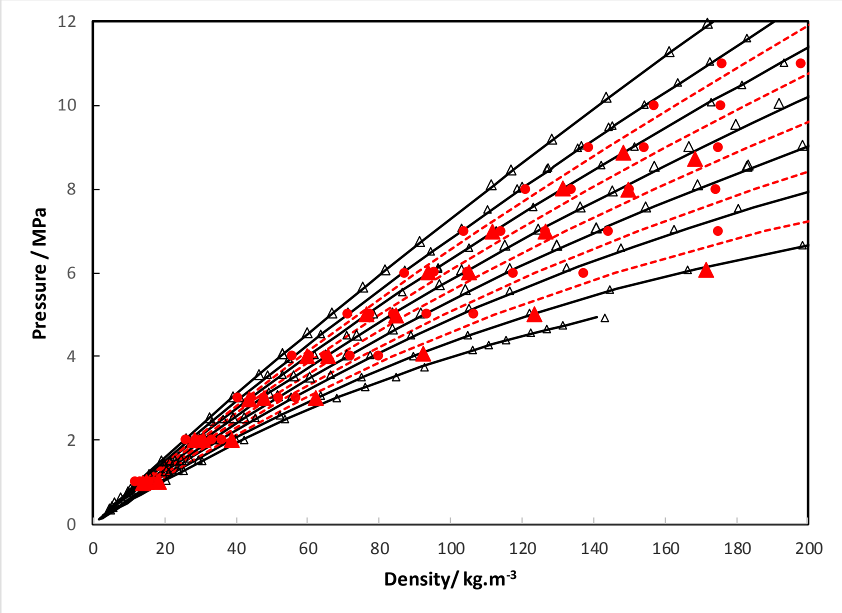

C

Figure 7: A: Pressure as a function of molar density for the O_2 + CO_2 (mixture 3: 0.128/0.872) binary system (C: zoom in the low pressure region). (Δ): this work. (●): Mantovani et al.[7], (▲): Lozano-Martin et al.[5] B: Compressibility factor as a function of pressure (Δ): 279.05 K, (×): 353.62 K, (▲):414.31 K. Solid and dashed line: Peng Robinson EoS with Wong Sandler mixing rules and NRTL Activity coefficient model.

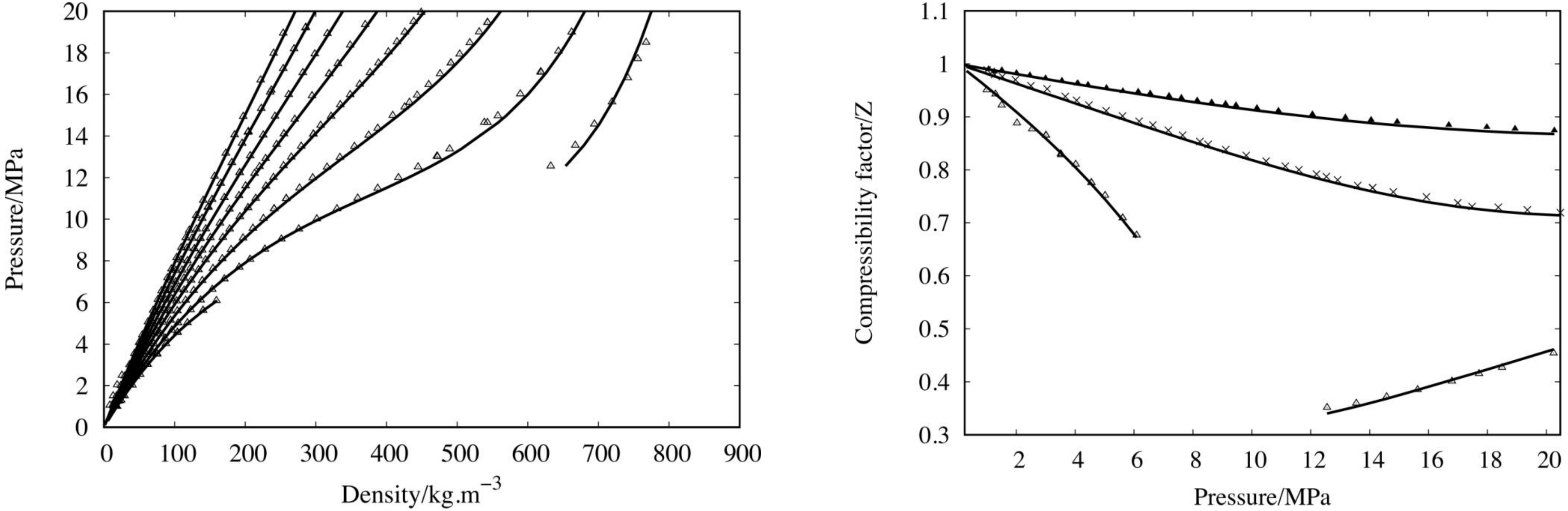

A B

Figure 8: A: Pressure as a function of density for the CO_2 + O_2 (mixture 1: 0.726/0.274) binary system. B: Compressibility factor as a function of pressure (Δ): 276. 50 K, (×): 353.78 K, (▲): 416.38 K. Solid line: EOS-CG.

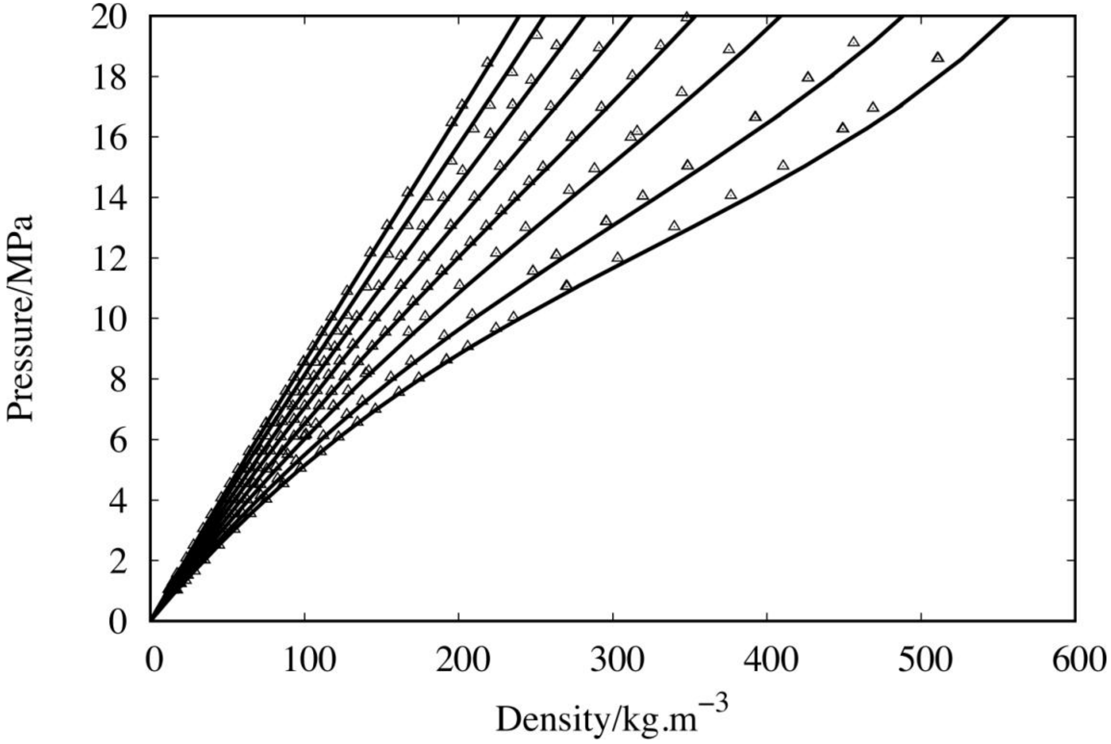

A

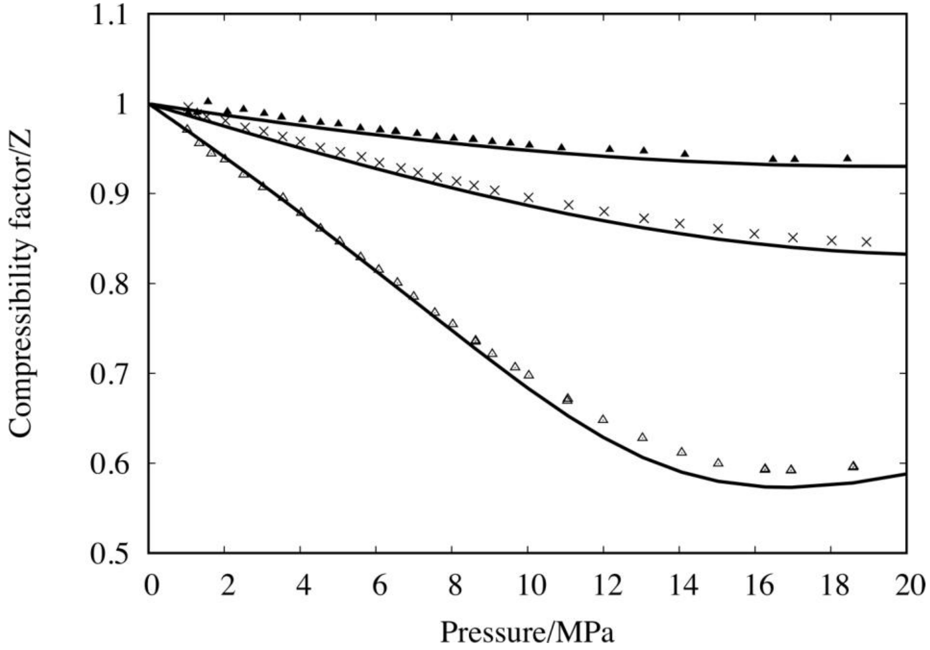

B

Figure 9: A: Pressure as a function of density for the CO_2 + O_2 (mixture 2: 0.517/0.483) binary system. B: Compressibility factor as a function of pressure (Δ): 280.63 K, (×): 353.46 K, (▲): 412.85 K. Solid line: EOS-CG.

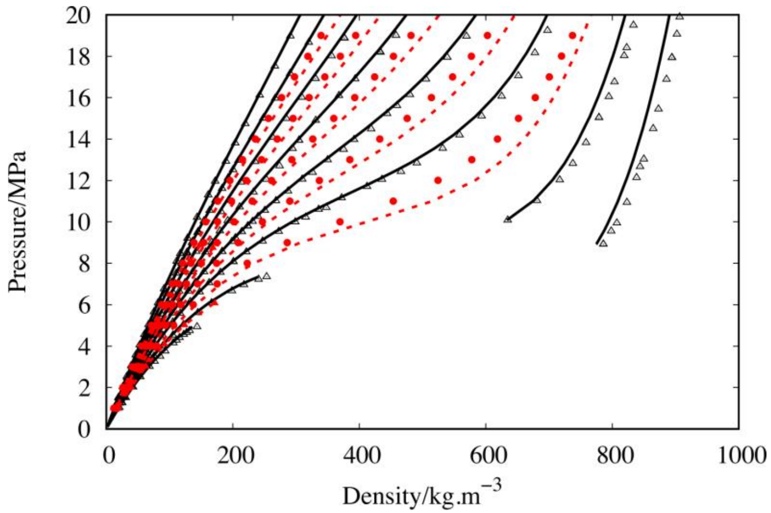

Pressure/MPa
Density/kg.m^{-3}
0
2
4
6
8
10
12
14
16
18
20
0
200
400
600
800
1000

A

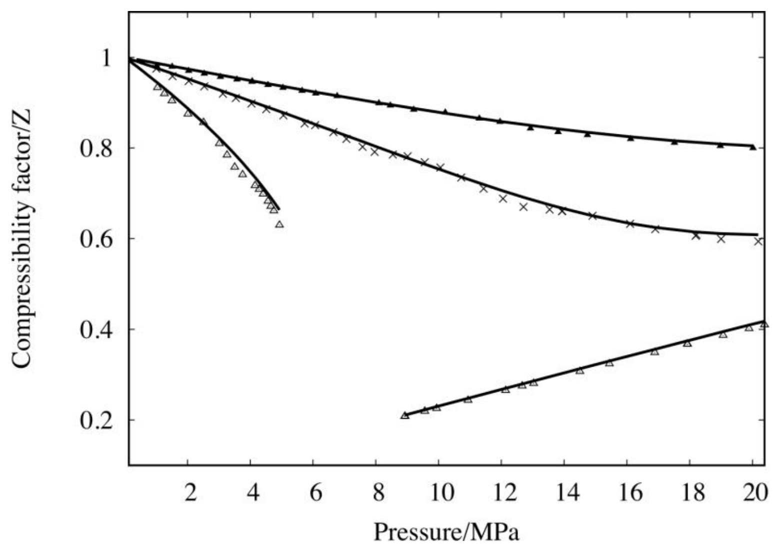

Compressibility factor/Z
Pressure/MPa
0.2
0.4
0.6
0.8
1
2
4
6
8
10
12
14
16
18
20

B

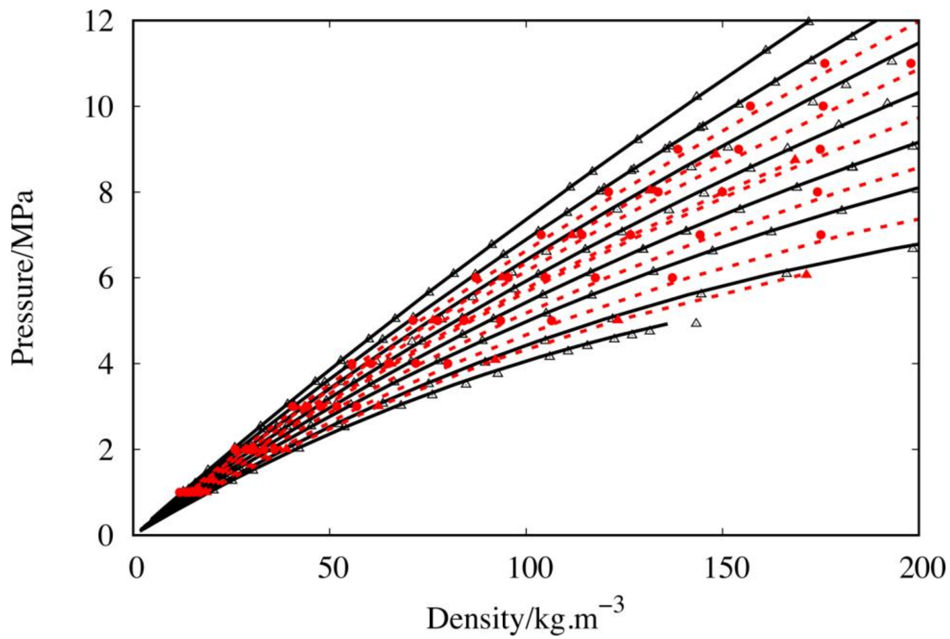

C

Figure 10: A: Pressure as a function of density for the CO_2 + O_2 (mixture 3: 0.872/0.128) binary system (C: zoom in the low pressure region). (∆): this work. (•): Mantovani et al.[7], (▲): Lozano-Martin et al.[5] B. B: Compressibility factor as a function of pressure (∆): 279.05 K, (×): 353.62 K, (▲): 414.31 K. Solid line: EOS-CG.

Experimental density data were also compared to a recent EoS, EOS-CG, based on GERG-2008[4, 15]. Parameters for the reduced mixture density and inverse reduced mixture temperature are provided by Gernert and Span[8], but the weighting factor F_{ij} is set to 0 for the binary system CO_2-O_2. As a result, the residual mixture behavior only includes the residual behavior of the pure components, weighted by their molar fraction. The reducing functions for density and temperature are presented in Eqs. (11) and (12), where N is the number of components, $T_{C,i}$ is the critical temperature of component i and $\rho_{C,i}$ is the critical density of component i.

$$\frac{1}{\rho_r(\bar{x})} = \sum_{i=1}^{N} x_i^2 \frac{1}{\rho_{c,i}} + \sum_{i=1}^{N-1}\sum_{j=i+1}^{N} 2x_i x_j \beta_{v,ij}\gamma_{v,ij} \frac{x_i+x_j}{\beta_{v,ij}{}^2 x_i + x_j} \cdot \frac{1}{8}\left(\frac{1}{\rho_{c,i}{}^{\frac{1}{3}}} + \frac{1}{\rho_{c,j}{}^{\frac{1}{3}}}\right)^3 \tag{11}$$

$$T_r(\overline{x}) = \sum_{i=1}^{N} x_i^2\, T_{c,i} + \sum_{i=1}^{N-1} \sum_{j=i+1}^{N} 2\beta_{T,ij}\gamma_{T,ij} \cdot (T_{c,i} \cdot T_{c,j})^{0.5}\, x_i x_j \frac{x_i+x_j}{\beta_{T,ij}{}^2 x_i + x_j} \tag{12}$$

$\beta_{v,ij}$, $\gamma_{v,ij}$, $\beta_{T,ij}$ and $\gamma_{T,ij}$ are binary interaction parameters from GERG-2008[4, 15] and presented in Table 10 for the system CO_2-O_2.

As shown in Table 9, EoS-CG predicts the densities more accurately than the PR EoS developed in this work. It should be noted that EOS-CG is based on multi-fluid approximations and that different types of data ($P\rho T$, VLE, speed of sound, etc.) are used for the development of binary model parameters. Figures 8 - 10 compare experimental and predicted densities and compressibility factors. Due to the use of different data types, rather than only VLE as PR EoS, the phase equilibrium prediction is less accurate for EOS-CG than for PR EoS (see Figure 3). This is also influenced by the presence of a mixture critical point.

Finally, we have compared our experimental results with literature data for compositions similar to ours, i.e. mixture 3. We have plotted the literature data in Figures 7 and 10 (we have also included a zoom to better visualize the low-pressure region). Deviations between these data and PR EoS and EOS-CG are presented in Table 9. As can seen, the order of magnitude of the deviations between our models and experimental data (and our data and literature data) are very close. We can observe a good agreement between the different sets of data.

Table 9: Deviations between experimental and calculated data using Peng Robinson EoS with the Wong Sandler mixing rules involving NRTL activity coefficient model, and using EoS-CG. Vap: vapor phase, Liq: liquid phase and SC: supercritical region.

	Peng Robinson EoS						EoS-CG					
***T*/K**	***AAD*/% Vap**	***AAD*/% Liq**	***AAD*/% SC**	***MAD*% Vap**	***MAD*% Liq**	***MAD*% SC**	***AAD*/% Vap**	***AAD*/% Liq**	***AAD*/% SC**	***MAD*% Vap**	***MAD*% Liq**	***MAD*% SC**
Mixture 1												
276.59	4.2	3.2		10.1	3.8		0.7	1.3		2.2	3.3	
293.18			3.2			4.5			1.3			3.8
313.18			2.0			3.9			1.5			2.2
334.78			2.2			3.9			0.6			1.3
353.78			1.5			3.1			0.8			1.3
373.46			1.4			2.4			0.5			0.7
395.18			1.3			2.1			0.6			0.7
416.38			0.9			1.4			0.4			0.9
Mixture 2												
280.63			2.8			4.6			1.6			3.7
293.92			2.7			4.7			2.1			3.4
313.63			3.1			4.4			2.1			2.8
333.21			1.4			2.4			0.8			1.4
353.46			1.6			2.4			1.0			1.6
373.60			1.5			2.2			1.3			1.9
395.72			1.9			4.7			1.7			2.3
412.85			1.1			2.8			0.7			1.2
Mixture 3												
279.05	3.0	3.7		12.6	8.2		2.3	1.8		5.1	2.0	
293.31			3.7			8.9	2.2	1.7		5.0	2.1	
315.06			3.5			8.6			1.1			3.1
333.25			2.3			7.1			0.9			2.3
353.62			1.6			6.8			0.9			3.1

374.23	1.4	4.5	1.7	5.1
394.15	1.0	3.0	0.3	0.8
414.31	0.8	2.4	0.4	0.8
Lozano-Martín et al.[5], x_{O2}=0.099856 – Maximum pressure: 9 MPa				
293.07	1.94	3.1	0.3	0.8
349.92	1.78	2.5	0.2	0.3
374.91	1.28	1.7	0.07	0.2
Mantovani et al.[7], x_{O2}=0.1291 – Maximum pressure: 20 MPa				
303.22	3.86	9.96	5.1	13.6
323.18	3.57	6.29	4.0	6.5
343.15	3.34	7.55	3.4	7.1
363.15	3.02	8.20	3.0	7.8
383.14	3.76	15.18	3.6	14.8

Table 10: Values of EoS-CG[4] binary interaction parameters.

System	β_T	γ_T	β_v	γ_v
$CO_2 + O_2$	1.0	1.032	1.0	1.0845

4. Conclusion

The densities of three CO_2-O_2 binary mixtures were measured using VTD densitometer, Anton Paar DMA 512, in the gas, liquid and supercritical regions. The densitometer was first calibrated using pure CO_2 and the FPMC calibration technique. The maximum expanded uncertainties on temperature, pressure and densities are $U(p)$= 0.0005 MPa, $U(T)$= 0.3 K and $U(\rho)$= 15 kg.m^{-3}, respectively. The highest uncertainties were observed at very low pressure conditions in the gas phase or in the vicinity of the bubble point curve in the liquid phase. The measured densities were employed to evaluate the classical Peng-Robinson cubic EoS with parameters adjusted on VLE data from the literature. The model gives satisfactory results in the prediction of the volumetric properties in the typical conditions of storage in salt caverns. However, the GERG-2008-based EoS-CG was more accurate with AAD of only 1.1% and MAD of 5.1%. The main advantage of EOS based on a thermodynamic potential is that all thermodynamic properties of a mixture or pure substance can be consistently derived from the potential; these properties are needed in the assessment of cavern stability.

5. Acknowledgments

Financial support from Agence Nationale de la Recherche (ANR) through the project FluidSTORY (n° 7747, ID ANR-15-CE06-0015) is gratefully acknowledged.

6. References

1. Götz, M.; Lefebvre, J.; Mörs, F.; Koch, A. M.; Graf, F.; Bajohr, S.; Reimert, R.; Kolb, T., Renewable Power-to-Gas: A technological and economic review. *Renewable energy* **2016,** 85, 1371-1390.

2. Kezibri, N.; Bouallou, C., Conceptual design and modelling of an industrial scale power to gas-oxy-combustion power plant. *Int. J. Hydrogen Energy* **2017,** 42, (30), 19411-19419.

3. Blanco-Martín, L.; Rouabhi, A.; Hadj-Hassen, F., Use of salt cavern in the energy transition context: application to the Power-to-Gas– Oxyfuel process. SN *Appl. Sci.* **2020,** submitted.

4. Li, H.; Dong, B.; Yu, Z.; Yan, J.; Zhu, K., Thermo-physical properties of CO_2 mixtures and their impacts on CO2 capture, transport and storage: progress since 2011. *Appl. Energy* **2019**, 255, 113789.

5. Lozano-Martin, D.; Akubue, G.U.; Moreau, A.; Tuma, D.; Chamorro, C.R., Accurate experipmental (p, ρ, T) data of the (CO2+O2) binary system for the development of models for CCs processes. *J. Chem. Thermodyn*. **2020**, 150, 106210.

6. Commodore, J.A.; Deering, C.E.; Marriott, R.A., Volumetric properties and phase behavior of sulfur dioxide, carbon disulfide and oxygen in high-pressure carbon dioxide fluid. *Fluid Phase Equilib*. **2018**, 477, 30-39.

7. Mantovani, M.; Chiesa, P.; Valenti, G.; Gatti, M.; Consonni, S., Supercritical pressure-density-temperature measurements on CO2-N2, CO2-O2 and CO2-Ar binary mixtures. *J. Supercrit. Fluids* **2012,** 61-34-43.

8. Gernert, J.; Span, R., EOS–CG: A Helmholtz energy mixture model for humid gases and CCS mixtures. *J. Chem. Thermodyn.* **2016,** 93, 274-293.

9. Rivollet, F.; Jarne, C.; Richon, D., PρT and VLE for Ethane+ Hydrogen Sulfide from (254.05 to 363.21) K at Pressures up to 20 MPa. *J Chem. Eng. Data* **2005,** 50, (6), 1883-1890.

10. Coquelet, C.; Ramjugernath, D.; Madani, H.; Valtz, A.; Naidoo, P.; Meniai, A. H., Experimental measurement of vapor pressures and densities of pure hexafluoropropylene. *J Chem. Eng. Data* **2010,** 55, (6), 2093-2099.

11. Nazeri, M.; Chapoy, A.; Valtz, A.; Coquelet, C.; Tohidi, B., Densities and derived thermophysical properties of the 0.9505 CO2+ 0.0495 H2S mixture from 273 K to 353 K and pressures up to 41 MPa. *Fluid Phase Equilib.* **2016,** 423, 156-171.

12. Bouchot, C.; Richon, D., An enhanced method to calibrate vibrating tube densimeters. *Fluid phase Equilib.* **2001,** 191, (1-2), 189-208.

13. Khalil, W.; Coquelet, C.; Richon, D., High-pressure Vapor− Liquid equilibria, liquid densities, and excess molar volumes for the carbon dioxide+ 2-propanol system from (308.10 to 348.00) K. *J. Chem. Eng. Data* **2007,** 52, (5), 2032-2040.

14. Lemmon, E.; Bell, I. H.; Huber, M.; McLinden, M., NIST Standard Reference Database 23: Reference Fluid Thermodynamic and Transport Properties-REFPROP, Version 10.0, National Institute of Standards and Technology. **2018**. *URL http://www.nist. gov/srd/nist23. cfm*.

15. Span, R.; Wagner, W., A new equation of state for carbon dioxide covering the fluid region from the triple-point temperature to 1100 K at pressures up to 800 MPa. *J. Phys. Chem. Ref. Data* **1996,** 25, (6), 1509-1596.

16. Peng, D.-Y.; Robinson, D. B., A new two-constant equation of state. *IEC Fund.* **1976,** 15, (1), 59-64.

17. Wong, D. S. H.; Sandler, S. I., A theoretically correct mixing rule for cubic equations of state. *AIChE J.* **1992,** 38, (5), 671-680.

18. Renon, H.; Prausnitz, J. M., Local compositions in thermodynamic excess functions for liquid mixtures. *AIChE J.* **1968,** 14, (1), 135-144.

19. Fredenslund, A.; Sather, G., Gas-liquid equilibrium of the oxygen-carbon dioxide system. *J. Chem. Eng. Data* **1970,** 15, (1), 17-22.

20. Kaminishi, G.-i.; Toriumi, T., Gas-liquid equilibrium under high pressures. VI. Vapor-liquid phase equilibrium in the CO2-H2, CO2-N2, and CO2-O2 systems. *Kogyo Kagaku Zasshi* **1966,** 69, (2), 175-178.

21. Muirbrook, N.; Prausnitz, J., Multicomponent vapor-liquid equilibria at high pressures: Part I. Experimental study of the nitrogen—oxygen—carbon dioxide system at 0° C. *AIChE J.* **1965,** 11, (6), 1092-1096.

22. Zenner, G.H.; Dana, L.I Liquid-vapor equilibrium compositions of carbon dioxide-oxygen-nitrogen mixtures, Chemical engineering progress symposium series, 1963, 36-41.

23. Lasala, S.; Chiesa, P.; Privat, R.; Jaubert, J.-N., VLE properties of CO2–Based binary systems containing N2, O2 and Ar: Experimental measurements and modelling results with advanced cubic equations of state. *Fluid Phase Equilib.* **2016,** 428, 18-31.

24. Westman, S. F.; Stang, H. J.; Løvseth, S. W.; Austegard, A.; Snustad, I.; Ertesvåg, I. S., Vapor-liquid equilibrium data for the carbon dioxide and oxygen (CO2+ O2) system at the temperatures 218, 233, 253, 273, 288 and 298 K and pressures up to 14 MPa. *Fluid Phase Equilib.* **2016,** 421, 67-87.

TOC GRAPHIC

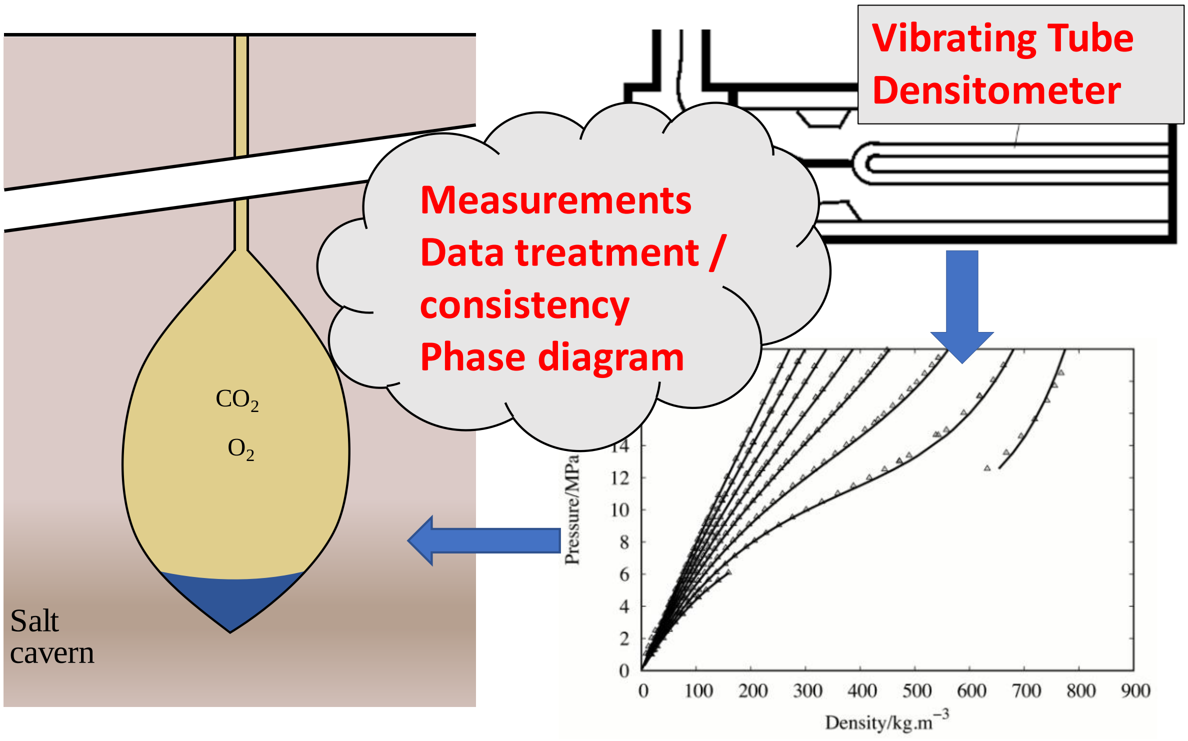
Vibrating Tube Densitometer
Measurements
Data treatment / consistency
Phase diagram
CO_2
O_2
Salt cavern
Pressure/MPa
Density/kg.m^{-3}
0 100 200 300 400 500 600 700 800 900
0 2 4 6 8 10 12 14